

# Confidence-Guided Radiology Report Generation

**Yixin Wang<sup>1,\*</sup>, Zihao Lin<sup>2,\*</sup>, Jiang Tian<sup>3</sup>, Zhongchao Shi<sup>3</sup>, Yang Zhang<sup>3</sup>,  
Jianping Fan<sup>3,4</sup>, Zhiqiang He<sup>1,3</sup>**

<sup>1</sup>ICT, Chinese Academy of Sciences, <sup>2</sup>Duke University, <sup>3</sup>Lenovo, <sup>4</sup>UNC Charlotte

wangyixin19@mails.ucas.ac.cn, z1293@duke.edu

{tianjiang1, shizc2, zhangyang20, hezq}@lenovo.com, jfan@uncc.edu

## Abstract

Medical imaging plays a pivotal role in diagnosis and treatment in clinical practice. Inspired by the significant progress in automatic image captioning, various deep learning (DL)-based architectures have been proposed for generating radiology reports for medical images. However, model uncertainty (i.e., model reliability/confidence on report generation) is still an under-explored problem. In this paper, we propose a novel method to explicitly quantify both the visual uncertainty and the textual uncertainty for the task of radiology report generation. Such multi-modal uncertainties can sufficiently capture the model confidence scores at both the report-level and the sentence-level, and thus they are further leveraged to weight the losses for achieving more comprehensive model optimization. Our experimental results have demonstrated that our proposed method for model uncertainty characterization and estimation can provide more reliable confidence scores for radiology report generation, and our proposed uncertainty-weighted losses can achieve more comprehensive model optimization and result in state-of-the-art performance on a public radiology report dataset.

## 1 Introduction

Radiology report generation, which combines Computer Vision (CV) and Natural Language Processing (NLP) to automatically generate reports for medical images, has become a rapidly-growing topic. Since hand-crafted diagnostic reports are very time-consuming and prone to both inter-rater and intra-rater variations, automatic generation may bring great benefits to doctors who are occupied with such work. With the convincing performance and understandable interpretations of AI's predictions, it is greatly potential to automate the clinic workflows. Existing researches for radiology report generation usually borrow ideas from natural image captioning [14, 31, 37, 19, 3, 6], where the images are firstly encoded to vectorial representations and then decoded to generate the captions.

Even promising results obtained, the reliability of the underlying DL models has not been explored sufficiently and no much attention has been paid to this reliability issue due to the following reasons. First, learning from inadequate samples may result in unreliable models, which may easily generate wrong reports. Second, the existing evaluation metrics are mostly designed for the NLP tasks, and they are proven to be insufficient [25, 17] for the task of generating radiology reports from medical images. Therefore, it is highly desirable to assess how much patients and doctors can trust such generated radiology reports on decision making. This motivates us to present a comprehensive confidence measurement to quantify the model uncertainty in radiology report generation.

---

\* Equal Contribution.

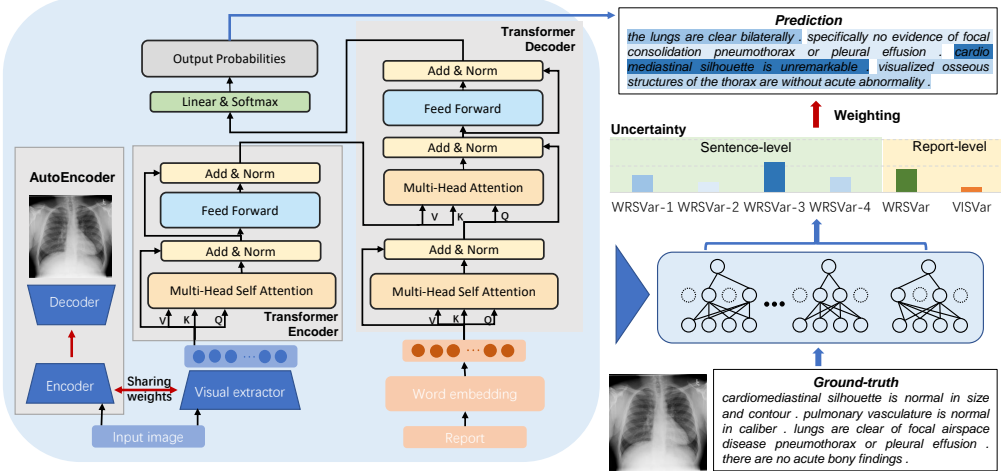


Figure 1: Illustration of our method. The left part shows that our network consists of an AutoEncoder for image reconstruction, a transformer encoder to extract features and a transformer decoder to predict words via attention mechanism. The right part shows our uncertainty estimation workflow.

Most existed researches on model uncertainty characterization focused on single-modal. [16, 1, 15, 12, 39] studied the model uncertainties for the classification/segmentation tasks, where additional supervisions are leveraged to promote the model’s prediction reliability. [34, 35] quantified the uncertainties for different NLP tasks, such as sentiment analysis, named entity recognition, language modeling and summarization. For multi-modal generation tasks, the uncertainties may appear in the processes for visual feature extraction and text generation, but estimating such multi-modal uncertainty is still unexplored because it is significantly different from single-modal ones.

In this paper, we propose a new method to characterize and quantify both of the visual and textual uncertainties in radiology report generation. We first adopt Monte Carlo (MC) dropout [8] to sample weights as a Bayesian Neural Network (BNN). Since it is unrealistic to directly quantify the model uncertainty for visual extraction in the output space, we then design an extra AutoEncoder to obtain such visual uncertainty, **VISVar**, which can estimate the parameter variance for the visual extractor and enhance the model to learn meaningful and generalizable latent representations. For the generated radiology reports, inspired by Word Rotator’s Distance (WRD) [38], we propose an Adjusted WRS Score (AdjWRS) to measure their similarities and **WRSVar** and **WRSVar-l** are further proposed to separately measure the model uncertainties at both the report-level and the sentence-level. Particularly, both these uncertainty measurements focus on the meanings of the sentences rather than their forms, which can provide more valuable confidence scores for the generated radiology reports. Finally, such visual-textual uncertainties are leveraged to define an uncertainty-weighted loss to achieve more comprehensive model optimization, lessen misjudgement risk and improve overall performance on radiology report generation. Our extensive experiments conducted on the Indiana University chest X-Ray (IU X-Ray) have demonstrated that our proposed method can achieve the state-of-the-art performance, and more important, it can characterize the visual-textual uncertainties more comprehensively and provide more reliable confidence scores for radiology report generation.

## 2 Related Work

**Radiology Report Generation:** For a given medical image, radiology report generation aims at automatically generating a set of descriptive and informative sentences. It is related to the computer vision task for image captioning, where various CNN-RNN/LSTM architectures together with attention mechanisms have achieved promising results [29, 36, 40, 24]. Recently, inspired by their capacity on parallel training, transformers [5, 42, 20, 10] have been successfully applied to predict words according to the extracted features from CNN. Generating radiology reports is much more challenging as it requires to identify the relevant information from noisy X-Ray images with similar patterns and generating long contextual descriptions [14, 31, 37, 19, 3, 6]. Particularly, Liu et al. [23] proposed a domain-aware automatic generation system, which employed a hierarchical

convolutional-recurrent neural network and reinforcement learning for report generation. Chen et al. [6] incorporated the relational memory into the transformer via a relational memory and memory-driven conditional layer normalization, which is capable of generating long reports with informative content and has achieved the state-of-the-art results. However, these methods only focus on achieving higher generation accuracy, but they do not actually evaluate whether the generated reports are reliable enough in clinical practice.

**Uncertainty Modeling:** Uncertainty mostly occurs due to the inadequate knowledge and data during model training, and uncertainty estimation is a key approach to quantify the reliability of the model’s predictions. BNN interprets a posterior uncertainty of the underlying model parameters, which can be realized via sampling weights and forwarding the inputs through the networks for multiple times. Recently, there are increasing numbers of studies on investigating the uncertainty in different CV and NLP tasks. These methods mostly quantify the uncertainties through the predicted classes such as segmentation [12, 39, 32], detection [18, 9], classification [15, 28], sentiment analysis and named entity recognition [34]. Machine translation or other text generation tasks usually quantify the uncertainties through Beam Score, Sequence Probability [30] or BLEU Score [33].

Compared with the above tasks, radiology reports generation is more tough because it relies on the uncertainties for both visual extraction and text generation. What’s more, most aforementioned uncertainty quantification methods for text generation are based on n-gram form of expressions. However, we need to pay more attention on the completeness and accuracy of generated reports. It is a promising direction as the uncertainty can provide information on how confident the generated reports are and in turn enables time-effective corrections by AI diagnosis itself and doctors.

### 3 Our Proposed Method

Figure 1 shows an overview of our proposed method. We first elaborate the image-text generation network in Section 3.1-3.3. Section 3.4 describes how to estimate the report-level and sentence-level uncertainties in our architecture. We then explain our novel uncertainty-weighted loss in Section 3.5.

#### 3.1 Feature AutoEncoder

The raw images are taken as the input  $\{\mathbf{X}\}_{i=1}^N \in \mathcal{R}^{3 \times 224 \times 224}$  for the image encoder, which serves as a feature extractor to obtain high-dimensional visual features to detect a wide range of visual concepts, landmarks and other entities for the language model. The image encoder is basically a pre-trained Convolution Neural Network (CNN) from ImageNet [7], and the parameters are fixed during training. However, entirely distinguished from natural images, X-ray images contain more specific physiological structures and composition. Since text generation largely relies on the content of the input images, the extracted features should be some specific X-ray features for a final description.

For the above purposes, we design an auxiliary AutoEncoder branch to add an additional guidance to the feature extractor for image reconstruction. This allows us to adjust the parameters of the encoder in order to extract the features that are more effective in addressing the target-specific problem. Considering the dataset is inadequate, this also brings regularization to the whole framework. Specifically, a shared encoder, which is pre-trained on Resnet-101, maps  $\mathbf{X}$  to hidden representations  $\mathbf{R} \in \mathcal{R}^{2048 \times 7 \times 7}$ . To preserve more spatial content, the feature maps from the intermediate layer are picked for the decoder part of AutoEncoder, with the size of  $\mathbf{Y} \in \mathcal{R}^{512 \times 28 \times 28}$ . We denote the mapping function  $f(\cdot)$  as

$$\mathbf{Y} = f(\mathbf{X}) = s_f(W\mathbf{X} + b_{\mathbf{X}}), \quad (1)$$

where  $s_f$  is a nonlinear activation function and  $W$  and  $b$  represent the weight matrix and bias. The decoder part of AutoEncoder is trained to reconstruct  $V$  back to  $X'$  via a mapping  $g(\cdot)$  as

$$\mathbf{X}' = g(\mathbf{Y}) = s_g(W'\mathbf{Y} + b_{\mathbf{Y}}). \quad (2)$$

The whole process is performed in an unsupervised manner which empowers the encoder with strong ability on automatic feature extraction. The reconstruction loss is generally a mean squared error (MSE) as

$$\ell_{AutoEn}(\theta) = \sum_{i=1}^N \|\mathbf{X}_i - \mathbf{X}'_i\|^2 = \sum_{i=1}^N \|\mathbf{X}_i - g(f(\mathbf{X}_i))\|^2. \quad (3)$$

### 3.2 Transformer Encoder

The obtained abundant task-specific features  $\mathbf{R}$  are then used as  $N$  input tokens with  $d$  dimensions to a standard transformer encoder. Each encoder layer consists of a multi-head self-attention layer followed by a positional feed-forward neural network. Specifically, the tokens are first transformed into query  $Q \in \mathcal{R}^{N_q \times d_k}$ , key  $K \in \mathcal{R}^{N_k \times d_k}$  and value  $V \in \mathcal{R}^{N_k \times d_v}$  as

$$Q = \mathbf{R}W_Q, \quad K = \mathbf{R}W_K, \quad V = \mathbf{R}W_V, \quad (4)$$

where  $W_Q, W_K, W_V$  are the learnable projection matrices. Then the scaled dot-product attention is applied by each attention head  $head_i$  as

$$head_i = \text{Attention}(Q, K, V) = \text{Softmax}\left(\frac{QK^T}{\sqrt{D_k}}\right)V. \quad (5)$$

All the results of different heads are aggregated by a linear transformation  $W_O$  as

$$\text{MultiHead}(Q, K, V) = \text{Concat}(head_1, \dots, head_h)W_O. \quad (6)$$

Besides, the residual connections and layer normalization Norm are performed, and the feed-forward operation FFN is adopted in the end of each block. The output of the encoder is formalized as

$$\mathbf{R}_m = \text{Norm}(\mathbf{R} + \text{MultiHead}(Q, K, V)), \quad \mathbf{R}' = \text{Norm}(\mathbf{R}_m + \text{FFN}(\mathbf{R}_m)). \quad (7)$$

### 3.3 Transformer Decoder

The transformer decoder consists of a multi-head self-attention module and a multi-head cross-attention module. The former receives the embedding matrix of the current report and outputs the tokens  $\mathbf{h}_a = \{\mathbf{h}_1, \mathbf{h}_2, \dots, \mathbf{h}_A\}$  with length  $A$ . The output  $\mathbf{R}'$  of the encoder is utilized as the key and value to the multi-head cross-attention, with  $\mathbf{h}_a$  treated as the query. It can be formalized as

$$\mathbf{h}_m = \text{Norm}(\mathbf{h}_a + \text{MultiHead}(\mathbf{h}_aW_h, \mathbf{R}'W_{R'}, \mathbf{R}'W_{R'})). \quad (8)$$

Similar to the encoder,  $\mathbf{h}_m$  is processed by FFN and Norm as

$$\mathbf{h}' = \text{Norm}(\mathbf{h}_m + \text{FFN}(\mathbf{h}_m)). \quad (9)$$

The context vector is then fed into a linear layer and it is then used to predict the probability of words.

### 3.4 Uncertainty Estimation

The generated reports can be successfully derived from the aforementioned model. However, there is still no estimation about the reliability level of such predictions, which is a crucial reference for doctors to make further decisions. To tackle this problem, we propose a new method to evaluate the uncertainties of the generation system, which are defined as Visual Uncertainty **VISVar** and Textual Uncertainty **WRVar**. These two uncertainties quantify the model's uncertainty from the perspective of the processes of image embedding and word generation, respectively. To estimate this uncertainty, we adopt Monte Carlo (MC) Dropout variational inference method [8]. Particularly, any neural network with dropout can be viewed as a BNN which interprets the probability distribution over the model's parameters. With the dropout activated, the model uncertainties can be estimated by performing  $T$  stochastic forward passes on the model, which samples from the approximate posterior.

#### 3.4.1 Visual Uncertainty

Since it could be difficult to perform uncertainty quantification for the feature extractor in the output space, our proposed AutoEncoder branch serves as a guidance to obtain the uncertainty map for the input image. This model is extended into a BNN, which captures uncertainty through Bayesian posterior of the reconstruction regression task. The posterior predictive distribution  $p(\mathbf{X}' | \mathbf{X})$  of  $\theta$  can be appropriated as follows.

$$p(\mathbf{X}' | \mathbf{X}) = \int p(\mathbf{X}' | \theta, \mathbf{X})p(\theta | \mathbf{X})d\theta. \quad (10)$$

As this is intractable in deep networks, we apply dropout variational inference method [8] to acquire the approximation of the true posterior distribution. In particular, the dropout operation is utilized

after each non-linear layer of the shared part of the AutoEncoder as we expect to obtain the posterior distribution of the feature extractor in our report generation framework. Given an input, the dropout is enabled and the output predictive distributions are obtained through  $T$  times stochastic forwarding pass the network. By averaging  $T$  samples, the mean  $\mu'_{\text{VIS}}$  and the variance  $\sigma'^2_{\text{VIS}}$  are obtained as

$$\mu'_{\text{VIS}} = \bar{\mathbf{X}'} = \frac{1}{T} \sum_{t=1}^T \mathbf{X}'_t, \quad \sigma'^2_{\text{VIS}} = \frac{1}{T} \sum_{t=1}^T \left( \mathbf{X}'_t - \frac{1}{T} \sum_{t=1}^T \mathbf{X}'_t \right)^2. \quad (11)$$

In this way,  $\sigma'^2_{\text{VIS}}$  is obtained as an uncertainty map for the corresponding input. The overall visual uncertainty is defined as the mean over all pixels of  $\mathbf{X}$ , i.e.,  $\text{VISVar} = \overline{|\sigma'_{\text{VIS}}|}$ , which represents the report-level visual uncertainty value.

### 3.4.2 Textual Uncertainty

The textual uncertainty can be obtained by the variance of similarity scores between predictions and ground-truths. Recent research [33] adopted the variance of BLEU scores of the output samples as the uncertainty for neural machine translation (NMT) tasks. However, different from natural NMT tasks, X-ray reports have two inherent characteristics which invalidate BLEU scores (discussed in Section 4.2). First, the n-gram formats of the sentences tend to affect BLEU scores unduly. Second, the BLEU scores are not able to reflect the redundant and missing information.

In this paper, we propose a new method, called Adjusted Word Rotator's Similarity (AdjWRS), to evaluate the similarity between two reports. Our AdjWRS derives from Word Rotator's Distance (WRD) [38] which is based on Earth Mover's Distance (EMD) (also called Wasserstein distance) [11, 27]. Based on AdjWRS, we further propose **WRSVar** to measure the report-level textual uncertainty and **WRSVar-l** to measure the sentence-level textual uncertainty.

Intuitively, EMD measures the minimum energy consumption that is required to turn one pile of dirt to another. In WRD, a sequence of word vectors serves as the pile of dirt and the energy consumption is the transfer distance from one sentence to another per unit information transfer. Assume that the sentence  $S$  has word vectors  $\mathbf{w}_1, \mathbf{w}_2, \dots, \mathbf{w}_n$ , the sentence  $S'$  has word vectors  $\mathbf{w}'_1, \mathbf{w}'_2, \dots, \mathbf{w}'_m$ , and the cosine similarity  $d_{i,j}$  represents the distance between  $\mathbf{w}_i$  and  $\mathbf{w}'_j$ . We denote the optimal solution as  $\lambda_{i,j}$  which represents turning  $\lambda_{i,j}$  amount of information from  $\mathbf{w}_i$  to  $\mathbf{w}'_j$ . Thus, measuring the similarity between two sentences  $S$  and  $S'$  becomes an optimal problem and can be expressed as follows.

$$\begin{aligned} \text{WRD}(S, S') &= \min_{\lambda_{i,j} \geq 0} \sum_{i,j} \lambda_{i,j} d_{i,j} \quad \text{s.t.} \quad \sum_j \lambda_{i,j} = p_i, \quad \sum_i \lambda_{i,j} = q_j, \\ d_{i,j} &= 1 - \frac{\mathbf{w}_i \cdot \mathbf{w}'_j}{\|\mathbf{w}_i\| \times \|\mathbf{w}'_j\|}, \end{aligned} \quad (12)$$

where  $p_i$  and  $q_j$  represent the information contained in the words  $\mathbf{w}_i$  and  $\mathbf{w}'_j$ . Moreover, according to [38], the information contained in each sentence  $I_S, I_{S'}$  is obtained through summing the norm of each word vector.

$$p_i = \frac{\|\mathbf{w}_i\|}{I_S}, \quad I_S = \sum_{i=1}^n \|\mathbf{w}_i\|; \quad q_j = \frac{\|\mathbf{w}'_j\|}{I_{S'}}, \quad I_{S'} = \sum_{j=1}^m \|\mathbf{w}'_j\|. \quad (13)$$

The WRD describes the distance between two sentences, and we denote  $\text{WRS} = 1 - \text{WRD}$  as the similarity score between them.

In order to accurately calculate the distance between two reports  $R = (S_1, S_2, \dots, S_L)$  and  $R' = (S'_1, S'_2, \dots, S'_{L'})$ , where  $L$  and  $L'$  represent the numbers of sentences, we match their sentence pairs with the similar description through a function  $\text{MATCH}(\cdot)$ , which is realized by sorting WRS scores between each pair of their sentences. The word rotator's similarity between two reports  $R$  and  $R'$  is calculated by

$$\text{WRS}(R, R') = \frac{2}{L + L'} \sum_{S_i, S'_j} \text{MATCH}_{i,j} (\text{WRS}(S_i, S'_j)). \quad (14)$$

Based on the characteristics of radiology reports, we assume that each sentence conveys independent information in a given report. Thus, the inconsistency between  $L$  and  $L'$  reflects the redundant or missing information. To eliminate this negative impact, WRS is multiplied by a penalty item as

$$\text{AdjWRS}(R, R') = \text{WRS}(R, R') * \left(1 - \frac{|L - L'|}{\max(L, L')}\right). \quad (15)$$

With  $T$  samples generated by  $T$  times MC Dropout, the variance of each report can be calculated by

$$\hat{\sigma}_{\text{WRS}}^2 \approx \frac{1}{(T-1)!} \sum_{i=1}^T \sum_{j=i+1}^T \left( \text{AdjWRS}(R_{\theta_i}, R_{\theta_j}) - \frac{1}{(T-1)!} \sum_{p=1}^T \sum_{q=p+1}^T \text{AdjWRS}(R_{\theta_p}, R_{\theta_q}) \right)^2, \quad (16)$$

where  $R_{\theta_i}$  and  $R_{\theta_j}$  denote the outputs of the models with different parameters  $\theta_i$  and  $\theta_j$ . The report-level textual uncertainty for each report,  $\text{WRSVar} = |\hat{\sigma}_{\text{WRS}}|$ , along with  $\text{VISVar}$  represents the report-level uncertainty. To obtain the sentence-level uncertainty, we first find an average reference report among all  $T$  samples. The average report has the smallest distance with the rest of  $T-1$  samples [33]. Therefore, the reference report  $\tilde{R}$  can be obtained by

$$\tilde{R} = \arg \min_{R_{\theta_i}} \left( \sum_{\forall j \neq i}^T (1 - \text{AdjWRS}(R_{\theta_i}, R_{\theta_j})) \right). \quad (17)$$

Denote  $\tilde{S}_l$  as the  $l^{th}$  sentence in  $\tilde{R}$ , and  $S_{\theta_j, l}$  as the corresponding sentence in report  $R_{\theta_j}$  with  $\tilde{S}_l$ . The sentence-level uncertainty of the  $l^{th}$  sentence in the reference report is defined as  $\text{WRSVar-}l = |\hat{\sigma}_{\text{WRS-}l}|$ , where

$$\hat{\sigma}_{\text{WRS-}l}^2 \approx \frac{1}{T-1} \sum_{j \neq \text{ref}}^T \left( \text{AdjWRS}(\tilde{S}_l, S_{\theta_j, l}) - \frac{1}{T-1} \sum_{p \neq \text{ref}}^T \text{AdjWRS}(\tilde{S}_l, S_{\theta_p, l}) \right)^2. \quad (18)$$

### 3.5 Uncertainty Weighting

The existing models are typically optimized with respect to the generated reports in a batch, where each report and its sentences are equally contributed to the losses. However, as the radiology reports hold similar forming and the corresponding sentences describe the same X-Ray region, it is greatly potential to combine multiple objective losses for each report or sentences and perform a weighted sum of multiple reports in one batch/sentences in one report. Since this weight selection is pretty important but sensitive, our report-level and sentence-level uncertainties can be treated as Rep-weighting and Sen-weighting to learn how to balance this weighting optimally. Given a batch of X-Ray images  $\{\mathbf{X}\}_{r=1}^R$  and the their real reports  $\{\mathbf{R}^*\}_{r=1}^R$ , the overall loss can be weighted as

$$\begin{aligned} \ell(\{\mathbf{X}\}, \{\mathbf{R}^*\}) &= \lambda_{\text{AutoEn}} \ell_{\text{AutoEn}} + \ell_{\text{Rep}}, \\ \ell_{\text{Rep}} &= \sum_{r=1}^R \underbrace{\exp[-(\alpha |\hat{\sigma}_{\text{WRS}, r}| + \beta(\overline{\exp(\mu'_{\text{VIS}, r})} + |\sigma'_{\text{VIS}, r}|))]}_{\text{Rep-Weighting}} \sum_{l=1}^{L_r} \underbrace{\exp[-\gamma |\hat{\sigma}_{\text{WRS-}l, r}|]}_{\text{Sen-Weighting}} \ell_{\text{Sen}}(S_{r, l}, S_{r, l}^*), \end{aligned} \quad (19)$$

where  $\lambda_{\text{AutoEn}}$ ,  $\alpha$ ,  $\beta$  and  $\gamma$  are four values to adjust  $\ell_{\text{AutoEn}}$  and the uncertainty weights,  $\beta(\cdot)$  denotes the mean over all pixels,  $S_{r, l}$  and  $S_{r, l}^*$  represent the  $l^{th}$  sentence in the  $r^{th}$  generated report and the corresponding ground-truth report in the batch,  $\ell_{\text{Sen}}$  calculates their cross entropy loss. This mechanism enables the model to learn an optimized set of weights for each sentence and each report. Higher  $|\hat{\sigma}_{\text{WRS}, r}|$  and  $|\sigma'_{\text{VIS}, r}|$  uncertainty value will decrease the contribution of  $r^{th}$  report and higher  $|\hat{\sigma}_{\text{WRS-}l, r}|$  leads to lower weighting of  $l^{th}$  sentence in all  $L_r$  sentences.

## 4 Experimental Results

The experiments are conducted based on Pytorch and an NVIDIA Tesla V100 32GB GPU with a frequently used public radiography dataset: the Indiana University chest X-Ray (IU X-Ray). It

consists of 7,470 chest X-ray images with 3,955 reports. We apply the same way as [6] to divide the entire data into train/validation/test as 7:1:2. Targeting at medical domain, we adopt a 200-dimensional word embedding BioWordVec [41] trained by fastText [4] as pre-trained vectors to calculate AdjWRS. For a fair comparison with other transformer-based methods, we set the transformer as three blocks, 8 heads and 512 hidden units as in [6]. The hyper-parameters are all set to 1 according to the best performance on the validation set. All the models are trained for 50 epochs and the best results are reported based on the validation set. Stochastic dropout with  $p = 0.5$  is applied for  $T = 10$  times. All the models are evaluated by BLEU [26], METEOR [2] and ROUGE-L [22].

#### 4.1 Performance Comparison

Table 1 shows the quantitative results of our proposed methods. First, we illustrate the effectiveness of our AutoEncoder and two weighting methods separately. "BASE" represents the vanilla transformer architecture for image captioning. It is observed that the "AutoEncoder" enhances the performance on all the metrics for the highest 7.5%, which suggests that the AutoEncoder brings stronger ability for feature extraction. Note that applying "Rep-Weighting" and "Sen-Weighting" can provide a large improvement, especially on BLEU-4 score. This indicates that using uncertainty to weight the loss can effectively optimize the process for reports/sentences generation.

"OURS" represents the combination of all of the aforementioned strategies. It outperforms the state-of-the-art approaches, such as COATT [14], HRGR-Agent [21], CMAS-RL [13] and M-D Transformer [6]. The qualitative results are shown in Figure 2. It suggests three cases including one normal radiology image (first line) and two images with some abnormalities (second & third lines). In the first case, our model achieves the best ability to describe each region and generates more accurate and professional expressions, such as "*cardiomedastinal silhouette*", "*osseous structures*" and "*normally inflated*". The other two images contain abnormalities about "*degenerative spine*" and "*low lung volumes*", which can also be better captured by our models.

Model	Evaluation Metrics					
	BLEU-1	BLEU-2	BLEU-3	BLEU-4	METEOR	ROUGE-L
BASE	0.405	0.257	0.184	0.141	0.169	0.349
+ AutoEncoder	0.435	0.272	0.194	0.147	0.171	<b>0.375</b>
+ AutoEncoder + Rep-Weighting	0.466	0.302	0.221	<b>0.173</b>	0.185	0.366
+ AutoEncoder + Sen-Weighting	<b>0.470</b>	<b>0.304</b>	<b>0.222</b>	0.171	<b>0.187</b>	0.366
COATT [14] <sup>†</sup>	0.455	0.288	0.205	0.154	-	0.369
HRGR-Agent [21] <sup>†</sup>	0.438	0.298	0.208	0.151	-	0.322
CMAS-RL [13] <sup>†</sup>	0.464	0.301	0.210	0.154	-	0.362
M-D Transformer [6] <sup>†</sup>	0.470	0.304	0.219	0.165	0.187	<b>0.371</b>
M-D Transformer [6] <sup>‡</sup>	0.454	0.289	0.211	0.165	0.180	0.358
<b>OURS</b>	<b>0.481</b>	<b>0.309</b>	<b>0.223</b>	<b>0.169</b>	<b>0.193</b>	0.365

Table 1: Comparison results. <sup>†</sup> refers to results from the original papers. <sup>‡</sup> refers to our reproduction results from officially released codes.

#### 4.2 Report-level & Sentence-level Uncertainty

**AdjWRS v.s. BLEU:** To illustrate the rationality of our textual uncertainty estimation, we first show that our proposed AdjWRS performs better than BLEU and WRS scores. We calculate the BLEU, WRS and AdjWRS scores between predictions and ground truth of 590 samples from testing set. To show the rationality of AdjWRS, we plot the AdjWRS and BLEU scores of each pair in Figure 3(a). One can easily observe that AdjWRS has a positive correlation with BLEU scores, which indicates that a more similar report tends to have a relatively higher AdjWRS score. It is also noted that the second plot in Figure 3(a) shows that when the BLEU scores of some reports pairs are equal to 0, their AdjWRS scores are still positive since AdjWRS is based on the contained medical information rather than the n-gram format. Figure 3(b) shows that AdjWRS can better reflect the information inconsistency. It tends to give lower scores if the predictions have redundant or missing sentences



Figure 2: Illustration of reports generated by BASE model, M-T Transformer and OURS. The left two columns are the input front and lateral chest X-ray images, followed by its ground-truth report.

compared with the ground-truths, while BLEU or WRS perform not so well. More comparisons of different evaluation metrics are discussed in Appendix A.1. Figure 3(c)(d) show three randomly selected reports A, B, C and two pair-wise similarities respectively, where AdjWRS outperforms BLEU scores on the precision of actual information rather than the n-gram format. Though differing largely in expressions, reports A and B give the same diagnosis. However, BLEU scores of A-B are much lower and indicate their high dissimilarity. Conversely, the AdjWRS score correctly shows their similarity. Moreover, C describes the evidence of disease which does not appear in A. Therefore, the similarity of A-C is supposed to be much lower than that of A-B. AdjWRS can reflect it while BLEU scores cannot.

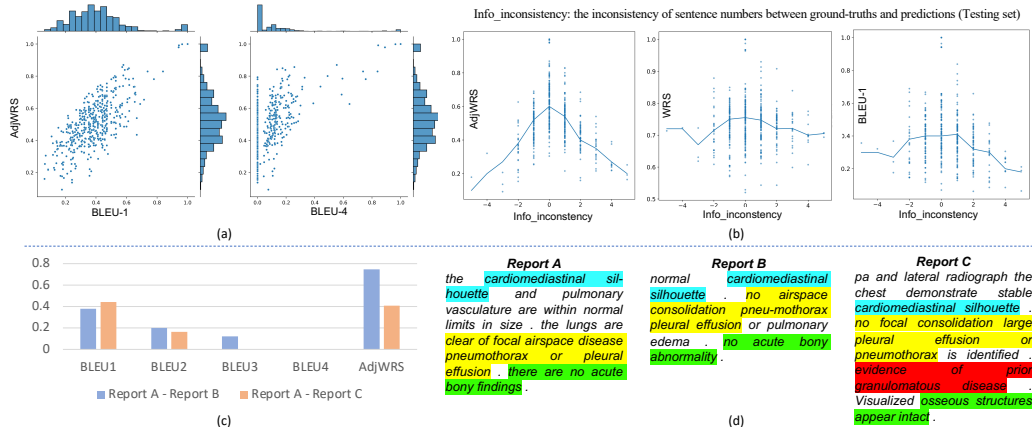


Figure 3: Comparison of AdjWRS and BLEU scores. a) Correlation between AdjWRS and BLEU scores. b) Relationship between similarity scores and information inconsistency. c) Comparison of different similarity scores of two reports pairs. (d) Compared reports.

**Report-level Uncertainty:** The report-level uncertainty is reflected by **WRSVar** and **VISVar**. We first draw a scatter plot from the testing set in Figure 5(a) to show the relationship among **WRSVar**, **VISVar** and BLEU-4 score. We set a threshold curve to find out the cases with extreme high uncertainty. The threshold can be modified based on doctors' risk assessment in clinical practice. This report-level uncertainty serves as an extra important evaluation to assess the reliability or

	Case	BLEU-4↑	VISVar↓	WRSVar↓
A	ground-truth: cardiac and mediastinal contours are within normal limits . the lungs are clear . bony structures are intact . prediction: the heart size and mediastinal silhouette are within normal limits for contour . the lungs are clear . no pneumothorax or pleural effusions . the xxxx are intact . stable left basilar atelectasis versus scarring .	0.239	0.047	0.274
B	ground-truth: the cardiomedastinal silhouette and pulmonary vasculature are within normal limits in size . the lungs are clear of focal airspace disease pneumothorax or pleural effusion . there are no acute bony findings . prediction: the lungs are clear bilaterally . specifically no evidence of focal consolidation pneumothorax or pleural effusion . cardio mediastinal silhouette is unremarkable . visualized osseous structures of the thorax are without acute abnormality .	0.210	0.035	0.209

Figure 4: Illustration of difference between BLEU-4 and report-level uncertainty.

confidence of the generated reports. Figure 4 shows two cases where A has a higher BLEU-4 score than B. However, the prediction of case A contains two redundant uncertain sentences and their **VISVar** and **WRSVar** show higher value than case B, which indicates the information contained in A is less confident than those in B. The superiorities of **VISVar** and **WRSVar** over AdjWRS are further discussed in Appendix A.2. It is also noted that if most generated sentences in one report are certain while only one is uncertain, **WRSVar** will still be lower. The proposed sentence-level uncertainty **WRSVar-l** can tackle this problem and measure each sentence’s uncertainty concisely.

**Sentence-level Uncertainty:** Figure 5(b)-(d) show the meanings of sentence-level uncertainty, where one case is presented, along with its several predictions  $MC - R_1$  to  $MC - R_T$  under  $T$  times MC dropout sampling and the reference report  $MC - \tilde{R}$  among them. Different colors represent the uncertainty values of the corresponding sentences. Our proposed reference report covers every information in the ground truth including lungs, pleural effusion, heart and spine with different uncertainties. One can easily observe that the sentence describing spine has the highest uncertainty, which can be explained through the uncertain predicted sentence on spine from  $MC - R_1$  to  $MC - R_T$ . This suggests that the model cannot make sure whether the spine is normal or not, which should be warned by report generation system and doctors to make further decisions.

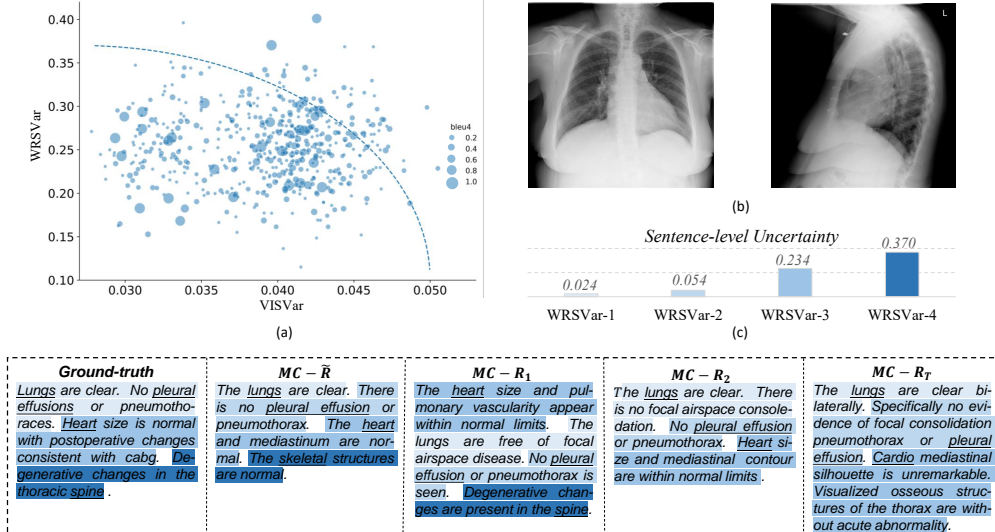


Figure 5: Illustration of the report-level and sentence-level uncertainties. a) The relationship among **WRSVar**, **VISVar** and BLEU-4. b) Front and lateral chest X-ray images. c) Sentence-level uncertainty. d) Ground-truth, reference report  $MC - \tilde{R}$ , and several MC outputs.

## 5 Conclusion

In this paper, a novel method is developed to explicitly quantify the model uncertainties (both the visual uncertainty and the textual uncertainty) for the task of radiology report generation. Such multi-modal uncertainty measurements can sufficiently capture the model confidence scores at both the report-level and the sentence-level and thus they are further leveraged to weight the losses to

achieve more comprehensive model optimization. Our experimental results have demonstrated that our proposed method can achieve the state-of-the-art performance and outperform the existing approaches.

At present, our model only builds relationships between the visual and textual uncertainties at the report-level. We intend to explicitly map the sentence-level uncertainty with the region-specific uncertainty in images, which will improve the model performance significantly, lead to better model interpretability, and provide better guidance in clinical practice. Future works also include introducing more prior knowledge from medical domain to enhance the reliability of the generation models.

## References

- [1] Moloud Abdar, Farhad Pourpanah, Sadiq Hussain, Dana Rezazadegan, Li Liu, Mohammad Ghavamzadeh, Paul Fieguth, Xiaochun Cao, Abbas Khosravi, U Rajendra Acharya, Vladimir Makarenkov, and Saeid Nahavandi. A review of uncertainty quantification in deep learning: Techniques, applications and challenges, 2021.
- [2] Satanjeev Banerjee and Alon Lavie. Meteor: An automatic metric for mt evaluation with improved correlation with human judgments. In *Proceedings of the acl workshop on intrinsic and extrinsic evaluation measures for machine translation and/or summarization*, pages 65–72, 2005.
- [3] William Boag, Tzu-Ming Harry Hsu, Matthew Mcdermott, Gabriela Berner, Emily Alesentzer, and Peter Szolovits. Baselines for Chest X-Ray Report Generation. In Adrian V. Dalca, Matthew B.A. McDermott, Emily Alsentzer, Samuel G. Finlayson, Michael Oberst, Fabian Falck, and Brett Beaulieu-Jones, editors, *Proceedings of the Machine Learning for Health NeurIPS Workshop*, volume 116 of *Proceedings of Machine Learning Research*, pages 126–140. PMLR, 13 Dec 2020.
- [4] Piotr Bojanowski, Edouard Grave, Armand Joulin, and Tomas Mikolov. Enriching word vectors with subword information. *Transactions of the Association for Computational Linguistics*, 5:135–146, 2017.
- [5] Ming Chen, Yingming Li, Zhongfei Zhang, and Siyu Huang. TVT: two-view transformer network for video captioning. In Jun Zhu and Ichiro Takeuchi, editors, *Proceedings of The 10th Asian Conference on Machine Learning, ACML 2018, Beijing, China, November 14-16, 2018*, volume 95 of *Proceedings of Machine Learning Research*, pages 847–862. PMLR, 2018.
- [6] Zhihong Chen, Yan Song, Tsung-Hui Chang, and Xiang Wan. Generating radiology reports via memory-driven transformer. In *Proceedings of the 2020 Conference on Empirical Methods in Natural Language Processing (EMNLP)*, pages 1439–1449, Online, November 2020. Association for Computational Linguistics.
- [7] Jia Deng, Wei Dong, Richard Socher, Li-Jia Li, Kai Li, and Li Fei-Fei. Imagenet: A large-scale hierarchical image database. In *2009 IEEE Conference on Computer Vision and Pattern Recognition*, pages 248–255, 2009.
- [8] Yarin Gal and Zoubin Ghahramani. Dropout as a bayesian approximation: Representing model uncertainty in deep learning. In Maria Florina Balcan and Kilian Q. Weinberger, editors, *Proceedings of The 33rd International Conference on Machine Learning*, volume 48 of *Proceedings of Machine Learning Research*, pages 1050–1059, New York, New York, USA, 20–22 Jun 2016. PMLR.
- [9] Yihui He, Chenchen Zhu, Jianren Wang, Marios Savvides, and Xiangyu Zhang. Bounding box regression with uncertainty for accurate object detection. In *2019 IEEE/CVF Conference on Computer Vision and Pattern Recognition (CVPR)*, pages 2883–2892, 2019.
- [10] Simao Herdade, Armin Kappeler, Kofi Boakye, and Joao Soares. Image captioning: Transforming objects into words. In Hanna M. Wallach, Hugo Larochelle, Alina Beygelzimer, Florence d’Alché-Buc, Emily B. Fox, and Roman Garnett, editors, *Advances in Neural Information Processing Systems 32: Annual Conference on Neural Information Processing Systems 2019, NeurIPS 2019, December 8-14, 2019, Vancouver, BC, Canada*, pages 11135–11145, 2019.

[11] F Hirzebruch N Hitchin L Hörmander, NJA Sloane B Totaro, and A Vershik M Waldschmidt. *Grundlehren der mathematischen wissenschaften* 332. 2006.

[12] Po-Yu Huang, Wan-Ting Hsu, Chun-Yueh Chiu, Ting-Fan Wu, and Min Sun. Efficient uncertainty estimation for semantic segmentation in videos, 2018.

[13] Baoyu Jing, Zeya Wang, and Eric Xing. Show, describe and conclude: On exploiting the structure information of chest X-ray reports. In *Proceedings of the 57th Annual Meeting of the Association for Computational Linguistics*, pages 6570–6580, Florence, Italy, July 2019. Association for Computational Linguistics.

[14] Baoyu Jing, Pengtao Xie, and Eric Xing. On the automatic generation of medical imaging reports. In *Proceedings of the 56th Annual Meeting of the Association for Computational Linguistics (Volume 1: Long Papers)*, pages 2577–2586, Melbourne, Australia, July 2018. Association for Computational Linguistics.

[15] Takafumi Kanamori, Akiko Takeda, and Taiji Suzuki. Conjugate relation between loss functions and uncertainty sets in classification problems. *Journal of Machine Learning Research*, 14(9):1461–1504, 2013.

[16] Alex Kendall and Yarin Gal. What uncertainties do we need in bayesian deep learning for computer vision? In I. Guyon, U. V. Luxburg, S. Bengio, H. Wallach, R. Fergus, S. Vishwanathan, and R. Garnett, editors, *Advances in Neural Information Processing Systems*, volume 30. Curran Associates, Inc., 2017.

[17] Mert Kilickaya, Aykut Erdem, Nazli Ikizler, and Erkut Erdem. Re-evaluating automatic metrics for image captioning. pages 199–209, 01 2017.

[18] Christian Leibig, Vaneeda Allken, Murat Seckin Ayhan, Philipp Berens, and Siegfried Wahl. Leveraging uncertainty information from deep neural networks for disease detection. *Scientific Reports*, 7, 12 2017.

[19] Christy Y. Li, Xiaodan Liang, Zhiting Hu, and Eric P. Xing. Hybrid retrieval-generation reinforced agent for medical image report generation, 2018.

[20] Guang Li, Linchao Zhu, Ping Liu, and Yi Yang. Entangled transformer for image captioning. In *2019 IEEE/CVF International Conference on Computer Vision, ICCV 2019, Seoul, Korea (South), October 27 - November 2, 2019*, pages 8927–8936. IEEE, 2019.

[21] Yuan Li, Xiaodan Liang, Zhiting Hu, and Eric P. Xing. Hybrid retrieval-generation reinforced agent for medical image report generation. In Samy Bengio, Hanna M. Wallach, Hugo Larochelle, Kristen Grauman, Nicolò Cesa-Bianchi, and Roman Garnett, editors, *Advances in Neural Information Processing Systems 31: Annual Conference on Neural Information Processing Systems 2018, NeurIPS 2018, December 3-8, 2018, Montréal, Canada*, pages 1537–1547, 2018.

[22] Chin-Yew Lin. Rouge: A package for automatic evaluation of summaries. In *Text summarization branches out*, pages 74–81, 2004.

[23] Guanxiong Liu, Tzu-Ming Harry Hsu, Matthew McDermott, Willie Boag, Wei-Hung Weng, Peter Szolovits, and Marzyeh Ghassemi. Clinically accurate chest x-ray report generation. In Finale Doshi-Velez, Jim Fackler, Ken Jung, David Kale, Rajesh Ranganath, Byron Wallace, and Jenna Wiens, editors, *Proceedings of the 4th Machine Learning for Healthcare Conference*, volume 106 of *Proceedings of Machine Learning Research*, pages 249–269, Ann Arbor, Michigan, 09–10 Aug 2019. PMLR.

[24] J. Lu, C. Xiong, D. Parikh, and R. Socher. Knowing when to look: Adaptive attention via a visual sentinel for image captioning. In *2017 IEEE Conference on Computer Vision and Pattern Recognition (CVPR)*, pages 3242–3250, 2017.

[25] Maram Mahmoud A. Monshi, Josiah Poon, and Vera Chung. Deep learning in generating radiology reports: A survey. *Artificial Intelligence in Medicine*, 106:101878, 2020.

[26] Kishore Papineni, Salim Roukos, Todd Ward, and Wei-Jing Zhu. Bleu: a method for automatic evaluation of machine translation. In *Proceedings of the 40th annual meeting of the Association for Computational Linguistics*, pages 311–318, 2002.

[27] Filippo Santambrogio. Optimal transport for applied mathematicians. *Birkhäuser, NY*, 55(58-63):94, 2015.

[28] Murat Sensoy, Lance Kaplan, and Melih Kandemir. Evidential deep learning to quantify classification uncertainty. In S. Bengio, H. Wallach, H. Larochelle, K. Grauman, N. Cesa-Bianchi, and R. Garnett, editors, *Advances in Neural Information Processing Systems*, volume 31. Curran Associates, Inc., 2018.

[29] O. Vinyals, A. Toshev, S. Bengio, and D. Erhan. Show and tell: A neural image caption generator. In *2015 IEEE Conference on Computer Vision and Pattern Recognition (CVPR)*, pages 3156–3164, 2015.

[30] Shuo Wang, Yang Liu, Chao Wang, Huanbo Luan, and Maosong Sun. Improving back-translation with uncertainty-based confidence estimation. *arXiv preprint arXiv:1909.00157*, 2019.

[31] X. Wang, Y. Peng, L. Lu, Z. Lu, and R. M. Summers. Tienet: Text-image embedding network for common thorax disease classification and reporting in chest x-rays. In *2018 IEEE/CVF Conference on Computer Vision and Pattern Recognition*, pages 9049–9058, 2018.

[32] Yixin Wang, Yao Zhang, Jiang Tian, Cheng Zhong, Zhongchao Shi, Yang Zhang, and Zhiqiang He. *Double-Uncertainty Weighted Method for Semi-supervised Learning*, pages 542–551. 09 2020.

[33] Tim Z Xiao, Aidan N Gomez, and Yarin Gal. Wat zei je? detecting out-of-distribution translations with variational transformers. *arXiv preprint arXiv:2006.08344*, 2020.

[34] Yijun Xiao and William Yang Wang. Quantifying uncertainties in natural language processing tasks. In *Proceedings of the AAAI Conference on Artificial Intelligence*, volume 33, pages 7322–7329, 2019.

[35] Jiacheng Xu, Shrey Desai, and Greg Durrett. Understanding neural abstractive summarization models via uncertainty. *arXiv preprint arXiv:2010.07882*, 2020.

[36] Kelvin Xu, Jimmy Ba, Ryan Kiros, Kyunghyun Cho, Aaron Courville, Ruslan Salakhudinov, Rich Zemel, and Yoshua Bengio. Show, attend and tell: Neural image caption generation with visual attention. In Francis Bach and David Blei, editors, *Proceedings of the 32nd International Conference on Machine Learning*, volume 37 of *Proceedings of Machine Learning Research*, pages 2048–2057, Lille, France, 07–09 Jul 2015. PMLR.

[37] Yuan Xue, Tao Xu, L. Rodney Long, Zhiyun Xue, Sameer K. Antani, George R. Thoma, and Xiaolei Huang. Multimodal recurrent model with attention for automated radiology report generation. In Alejandro F. Frangi, Julia A. Schnabel, Christos Davatzikos, Carlos Alberola-López, and Gabor Fichtinger, editors, *Medical Image Computing and Computer Assisted Intervention - MICCAI 2018 - 21st International Conference, Granada, Spain, September 16-20, 2018, Proceedings, Part I*, volume 11070 of *Lecture Notes in Computer Science*, pages 457–466. Springer, 2018.

[38] Sho Yokoi, Ryo Takahashi, Reina Akama, Jun Suzuki, and Kentaro Inui. Word rotator’s distance. In *Proceedings of the 2020 Conference on Empirical Methods in Natural Language Processing (EMNLP)*, pages 2944–2960, 2020.

[39] Lequan Yu, Shujun Wang, Xiaomeng Li, Chi-Wing Fu, and Pheng-Ann Heng. Uncertainty-aware self-ensembling model for semi-supervised 3d left atrium segmentation. In Dinggang Shen, Tianming Liu, Terry M. Peters, Lawrence H. Staib, Caroline Essert, Sean Zhou, Pew-Thian Yap, and Ali Khan, editors, *Medical Image Computing and Computer Assisted Intervention – MICCAI 2019*, pages 605–613, Cham, 2019. Springer International Publishing.

- [40] Hanwang Zhang, Jun Xiao, Liqiang Nie, Jian Shao, Wei Liu, and Tat-Seng Chua. Sca-cnn: Spatial and channel-wise attention in convolutional networks for image captioning. pages 6298–6306, 07 2017.
- [41] Yijia Zhang, Qingyu Chen, Zhihao Yang, Hongfei Lin, and Zhiyong Lu. Biowordvec, improving biomedical word embeddings with subword information and mesh. *Scientific data*, 6(1):1–9, 2019.
- [42] Luowei Zhou, Yingbo Zhou, Jason J. Corso, Richard Socher, and Caiming Xiong. End-to-end dense video captioning with masked transformer. In *2018 IEEE Conference on Computer Vision and Pattern Recognition, CVPR 2018, Salt Lake City, UT, USA, June 18-22, 2018*, pages 8739–8748. IEEE Computer Society, 2018.

## A Appendix

### A.1 Comparison of Different Evaluation Metrics

As mentioned in Section 3, this section provides with additional comparison of our proposed AdjWRS with different natural language generation (NLG) metrics: BLEU-n, ROUGE-L and METEOR. Figure 6 illustrates the relationships between them. Firstly, it is observed that AdjWRS has positive correlations with all the NLG metrics, which indicates the AdjWRS can correctly reflect the similarity between predictions and ground-truths. Secondly, it is irrational that the BLEU-2/3/4 of many predictions are equal to 0, as these n-gram-based methods focus more on the sentence format. Conversely, since AdjWRS is based on real medical meanings, their AdjWRS values will not be 0. Figure 7 shows that AdjWRS can better evaluate the information inconsistency than other metrics.

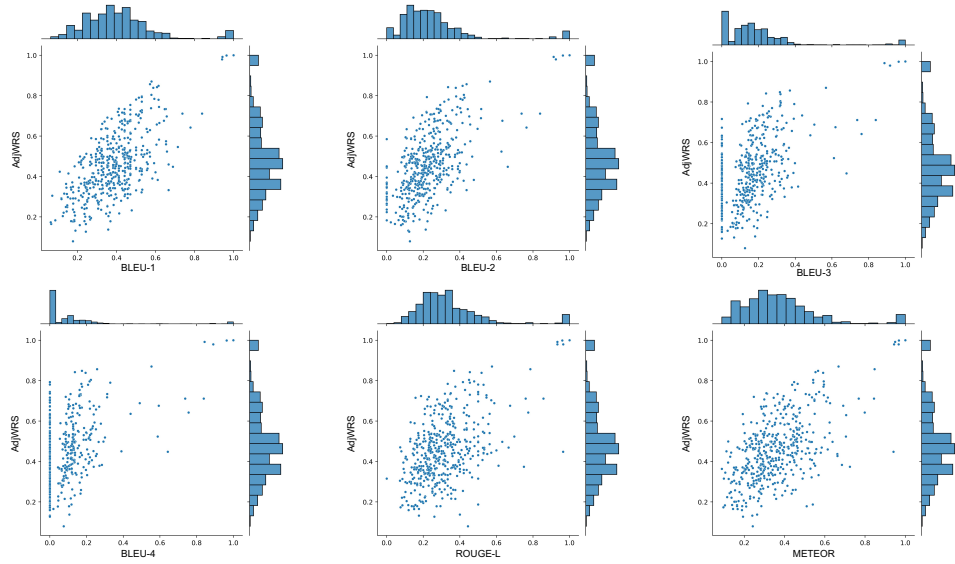


Figure 6: The relationships between AdjWRS and other NLG evaluation metrics. The metrics evaluate the predictions of 590 samples from the testing set.

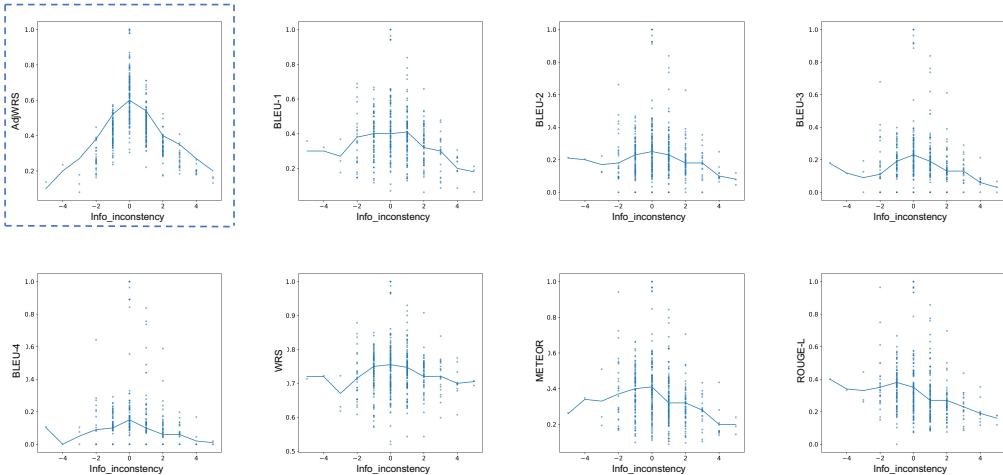


Figure 7: Relationships between similarity metrics and information inconsistency. ‘Info\_inconsistency’ represents the difference of sentence numbers. Positive/negative values indicate that the predictions have redundant/missing information, which should have lower similarity values than predictions with ‘0’ ‘info\_inconsistency’.

## A.2 Report-level Uncertainty Samples

We illustrate how **WRSVar** and **VISVar** serve as the confidence evaluation methods. Figure 8 shows three cases A, B and C, all of which are predicted correctly by the model. They have similar AdjWRS values as AdjWRS evaluates the results only from the similarity of ground-truths and predictions. However, due to the different input X-ray images, the model holds different confidence in their predictions, which can be captured by our methods in Table 2, 3, 4. With  $T = 10$  times MC dropout, the generated 10 predictions from the input images of case A are much uncertain while the 10 predictions are similar from B and C. Though A and B have the same AdjWRS, the MC-#1/#3/#6/#7 of case A include wrong information "*the heart and lungs have xxxx xxxx in the interval*", which makes the final prediction not as reliable as case B. Therefore, the **WRSVar** and **VISVar** of B are rather smaller than A, which means the model is more confident and certain in B's X-ray images.

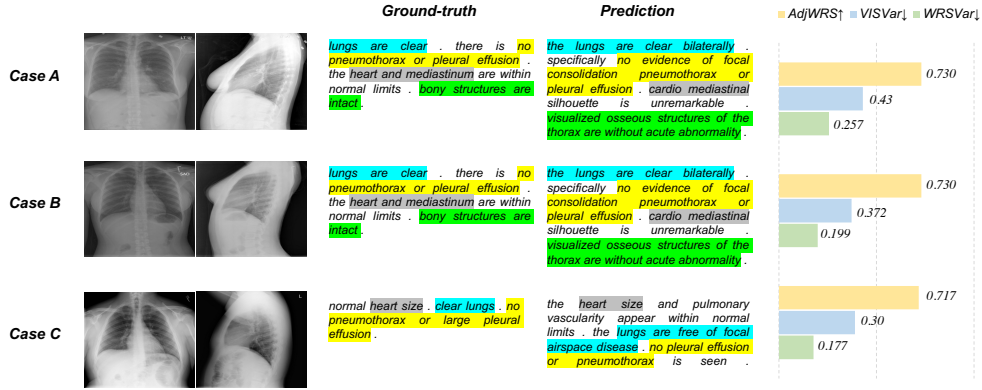


Figure 8: Samples of report-level uncertainties. Note that the value of **VISVar** is 10 times the real value for display. Lower **VISVar** and **WRSVar** and higher **AdjWRS** indicate better performance.

Case # MC Samples

A	1	<b>the heart and lungs have xxxx xxxx in the interval.</b> both lungs are clear and expanded. heart and mediastinum normal.
	2	the lungs are clear bilaterally. specifically no evidence of focal consolidation pneumothorax or pleural effusion. cardio mediastinal silhouette is unremarkable. visualized osseous structures of the thorax are without acute abnormality.
	3	<b>the heart and lungs have xxxx xxxx in the interval.</b> both lungs are clear and expanded. heart and mediastinum normal.
	4	the lungs are clear bilaterally. specifically no evidence of focal consolidation pneumothorax or pleural effusion. cardio mediastinal silhouette is unremarkable. visualized osseous structures of the thorax are without acute abnormality.
	5	the heart is normal in size. the mediastinum is unremarkable. the lungs are clear.
	6	<b>the heart and lungs have xxxx xxxx in the interval.</b> both lungs are clear and expanded. heart and mediastinum normal.
	7	<b>the heart and lungs have xxxx xxxx in the interval.</b> both lungs are clear and expanded. heart and mediastinum normal.
	8	the heart is normal in size. the mediastinum is unremarkable. the lungs are clear.
	9	the cardiomedastinal silhouette and pulmonary vasculature are within normal limits in size. the lungs are clear of focal airspace disease pneumothorax or pleural effusion. there are no acute bony findings.
	10	heart size within normal limits. no focal alveolar consolidation no definite pleural effusion seen. no typical findings of pulmonary edema. no pneumothorax.

Table 2: Generated  $MC$  predictions from case A under  $T = 10$  times  $MC$  dropout sampling. Wrong predictions are highlighted.

Case #	MC Samples
1	the heart size and mediastinal silhouette are within normal limits for contour . the lungs are clear . no pneumothorax or pleural effusions . the xxxx are intact.
2	the lungs are clear bilaterally . specifically no evidence of focal consolidation pneumothorax or pleural effusion . cardio mediastinal silhouette is unremarkable . visualized osseous structures of the thorax are without acute abnormality.
B	3 the heart is normal in size . the mediastinum is unremarkable . the lungs are clear. 4 lungs are clear . no focal consolidation effusion or pneumothorax . cardiomedastinal silhouette is within normal limits . no acute bony or soft tissue abnormality. 5 the heart size and mediastinal silhouette are within normal limits for contour . the lungs are clear . no pneumothorax or pleural effusions . the xxxx are intact. 6 the heart is normal in size . the mediastinum is unremarkable . the lungs are clear. 7 lungs are clear bilaterally . cardiac and mediastinal silhouettes are normal . pulmonary vasculature is normal . no pneumothorax or pleural effusion . no acute bony abnormality. 8 the lungs are clear bilaterally . specifically no evidence of focal consolidation pneumothorax or pleural effusion . cardio mediastinal silhouette is unremarkable . visualized osseous structures of the thorax are without acute abnormality. 9 the heart is normal in size . the mediastinum is unremarkable . the lungs are clear. 10 the lungs are clear . no focal airspace consolidation . no pleural effusion or pneumothorax . heart size and mediastinal contour are within normal limits.

Table 3: Generated  $MC$  predictions from case B under  $T = 10$  times  $MC$  dropout sampling.

Case #	MC Samples
1	the cardiomedastinal silhouette is within normal limits for size and contour. the lungs are normally inflated without evidence of focal airspace disease pleural effusion or pneumothorax. osseous structures are within normal limits for patient age.
C	2 lungs are clear. no pleural effusions or pneumothoraces. heart and mediastinum of normal size and contour. 3 the heart is normal in size. the mediastinum is unremarkable. the lungs are clear. 4 lungs are clear. no pleural effusions or pneumothoraces. heart and mediastinum of normal size and contour. 5 the cardiomedastinal silhouette is within normal limits for size and contour. the lungs are normally inflated without evidence of focal airspace disease pleural effusion or pneumothorax. osseous structures are within normal limits for patient age. 6 heart size and pulmonary vascularity appear within normal limits. the lungs are free of focal airspace disease. no pleural effusion or pneumothorax is seen. 7 cardiac and mediastinal contours are within normal limits. the lungs are clear. bony structures are intact. 8 the heart is normal in size. the mediastinum is unremarkable. the lungs are clear. 9 the heart is normal in size. the mediastinum is unremarkable. the lungs are clear. 10 the lungs are clear. no pleural effusions or pneumothoraces. heart and mediastinum of normal size and contour. degenerative changes in the spine.

Table 4: Generated  $MC$  predictions from case C under  $T = 10$  times  $MC$  dropout sampling.